Beam-Waveguide Antenna Servo Design Issues for Tracking Low Earth-Orbiting Satellites

W. K. Gawronski and J. A. Mellstrom
Ground Antennas and Facilities Engineering Section

Upcoming NASA missions will require tracking of low-orbit satellites. As a consequence, NASA antennas will be required to track satellites at higher rates than for the current deep space missions. This article investigates servo design issues for the 34-m beam-waveguide antennas that track low-orbit satellites. This includes upgrading the servo with a feedforward loop, using a monopulse controller design, and reducing tracking errors through either proper choice of elevation pinion location, application of a notch filter, or adjustment of the elevation drive amplifier gain. Finally, improvement of the signal-to-noise ratio through averaging of the oversampled monopulse signal is described.

I. Introduction

Future NASA missions will include low-orbiting satellites with significantly higher antenna tracking rates, as compared with the deep space missions. Thus, the JPL/NASA antenna servos should be upgraded to be able to follow commands at higher rates. A feedforward upgrade, discussed in [1], is the simple and reliable choice. For tracking, a monopulse controller is an alternative to the existing conscan tracking, since the former is much faster than the latter. The design and performance of a monopulse controller is discussed. It is shown that its performance can be improved through proper choice of the location of the elevation pinion, the implementation of a notch filter, or the adjustment of the amplifier gain. Finally, the improvement of the signal-to-noise ratio (SNR) of the monopulse signal is presented. By averaging the redundant monopulse samples, the SNR improvement is from 7 to 17 dB.

II. Feedforward Controller Design

Tracking accuracy of fast moving objects can be improved if a proportional-and-integral (PI) control system is augmented with a feedforward loop [1], shown in Fig. 1. In this diagram, G_p, G_c, G_f, and G_w denote transfer functions of the antenna's rate loop, PI controller, feedforward gain, and wind disturbance, respectively; r is a command; y is output (elevation and azimuth angles); e is tracking error in azimuth and elevation; u is plant input; and w is wind disturbance. Almost perfect tracking ($e \cong 0$) in the absence of disturbances is obtained for the feedforward gain G_f such that $G_f = j\omega I_2$, c.f., [1].

The closed-loop transfer function (elevation encoder to elevation command) for a system with and without the feedforward gain is compared in Fig. 2. The figure shows that for frequencies up to 1 Hz, the system with the feedforward gain has superior tracking properties as

compared with the system without feedforward gain. This is confirmed by tracking simulations with a trajectory, as in Fig. 3. The DSS-13 antenna, with proportional gain $k_p = 0.5$ and integral gain $k_i = 1.8$ in azimuth and elevation, was investigated. For the servo with the feedforward loop, the error of 1.4 mdeg in elevation and 0.2 mdeg in cross-elevation was observed, which exceeds the requirements. However, for this controller, the high-frequency components of the command are strongly amplified, as can be observed from the transfer function plots in Fig. 2, where the resonance peaks of the system with feedforward gain are much higher than the ones of the system without feedforward gain. As a result, any sharp change in the command may cause excessive vibrations of the antenna.

Despite the increased sensitivity to the command inputs, the disturbance rejection of the antenna with a feedforward loop remains the same as that for the antenna without a feedforward loop. Thus, the pointing errors due to wind gust disturbances are comparable to the results obtained for the DSS-13 antenna with the PI servo.

III. Monopulse Controller Design

In monopulse tracking, a deviation of an antenna from a target is detected by four slightly displaced feedhorns, each receiving the signal from a slightly different angle. The received beams are added and subtracted to form a sum and a difference beam. The difference beam is zero when the target is on the antenna boresight, and the nonzero difference beam produces an error signal, which is used by the monopulse control system. A detailed description of the monopulse technique is given in [2–5].

The monopulse tracking control system is shown in Fig. 4. It consists of the plant, the monopulse feedhorns, and the monopulse controllers in azimuth (H_a) and elevation (H_e). The plant in this case is the antenna with the closed encoder position loop. The monopulse feedhorns detect the tracking errors in azimuth (e_a) and elevation (e_e). The encoder command is denoted r_a in azimuth and r_e in elevation. The feedhorns detect the tracking errors e_a and e_e directly, and the output signals y_a and y_e, as well as the commands c_a and c_e, are not available. Note that y_a and y_e signals are not the encoder output, but the antenna positions related to the focal location of the RF beam.

Denote the two-input, two-output plant transfer function G

$$G = \begin{bmatrix} G_{aa} & G_{ae} \\ G_{ea} & G_{ee} \end{bmatrix} \tag{1}$$

and introduce the following notations:

$$c = \begin{bmatrix} c_a \\ c_e \end{bmatrix}, \; r = \begin{bmatrix} r_a \\ r_e \end{bmatrix}, \; e = \begin{bmatrix} e_a \\ e_e \end{bmatrix},$$

$$y = \begin{bmatrix} y_a \\ y_e \end{bmatrix}, \; H = \mathrm{diag}(H_a, H_e) \tag{2}$$

It follows from Fig. 4 that

$$y = G_c c + G_r r \tag{3}$$

where $G_c = (I + GH)^{-1}GH$ and $G_r = (I + GH)^{-1}G$ are of dimension 2×2

$$G_c = \begin{bmatrix} G_{caa} & G_{cae} \\ G_{cea} & G_{cee} \end{bmatrix}, \; G_r = \begin{bmatrix} G_{raa} & G_{rae} \\ G_{rea} & G_{ree} \end{bmatrix} \tag{4}$$

The components of G have the following properties

$$| G_{aa} | \cong | G_{ee} | \cong 1 \text{ for } f < f_o \tag{5a}$$

$$| G_{aa} | \ll 1, \; | G_{ee} | \ll 1 \text{ for } f \gg f_o \tag{5b}$$

$$| G_{ae} | \ll 1, \; | G_{ea} | \ll 1 \text{ for all } f \tag{5c}$$

as illustrated in Fig. 5. The above properties yield the following monopulse loop properties

$$y \cong c \text{ for } \| GH \| \gg 1 \tag{6a}$$

$$y \cong r \text{ for } \| GH \| \ll 1 \tag{6b}$$

$$y \cong 0.5(c + r) \text{ for } GH \cong I \tag{6c}$$

In the first case of large open-loop gain, the closed-loop monopulse system follows the monopulse command. In the second case of small open-loop gain, the closed-loop system follows the encoder command. In the last case of unit monopulse gain, the system follows the average of the monopulse and the encoder commands. In order to prove this, note that, for $\| GH \| \gg 1$, one obtains $\| G_r \| \ll 1$ and $\| G_c \| \cong I$, hence $y \cong c$; for $\| GH \| \ll 1$, one obtains $\| G_c \| \ll 1$ and $G_r \cong G$, thus $y \cong r$; for $GH \cong I$, one obtains $G_r \cong 0.5G$, thus, from Eq. (3),

$y = 0.5GHc + 0.5Gr$; and, since $G \cong I$ (see Eq. (5)), one obtains $y = 0.5(c + r)$.

The transfer function H of the monopulse controller is determined as follows. The monopulse bandwidth f_m is smaller than the encoder bandwidth f_o; therefore, the monopulse tracker will compensate for a slowly varying error signal e. If the condition presented in Eq. (6a) is satisfied for $f < f_m$, the monopulse tracking system will follow the command c. And since $G \cong I$ for $f < f_m$, $\| H \| \gg 1$ is required to satisfy the condition presented in Eq. (6a). In addition, a rapid roll-off rate for $f > f_m$ would be an advantage. However, the roll-off rate is limited through the Bode conditions, as specified in [6, p. 25]. Namely, the roll-off rate in the region of the gain crossover frequency must not exceed 40 dB/decade, and for a reasonable stability margin it must actually be smaller than this. Due to this restriction, the following transfer function of the monopulse tracker is chosen

$$H = \frac{2\pi f_m}{s} I_2 \tag{7}$$

This transfer function satisfies Eq. (6a) for $f < f_m$ and has a roll-off rate of 20 dB/decade for $f > f_m$ (see Fig. 5). The parameter f_m of H is determined by analyzing the root locus of the monopulse closed-loop system with respect to f_m. The plot of real parts of closed-loop poles is shown in Fig. 6. It shows that for $f_m \geq 0.067$ Hz, the monopulse system is unstable. In order to maintain a reasonable stability margin, $f_m = 0.04$ Hz is chosen.

The plant transfer function G is obtained for the DSS-13 antenna with the encoder loop closed and the feedforward loop implemented. The magnitudes of the plant transfer function are shown in Fig. 7. From the figure, one can see that the condition of Eqs. (5a) and (5b) are satisfied, but the condition of Eq. (5c) is violated for some frequencies from the interval $f = [2, 10]$ Hz. This violation will cause some performance deterioration.

The azimuth and elevation components of the command signal r are shown in Fig. 3. The command c is slightly deviated from r by δ, i.e., $c = r + \delta$, where $\| \delta \| \ll \| r \|$. The plot of δ is shown in Fig. 8. Magnitudes of the transfer functions are shown in Fig. 9 from input r to output y, and in Fig. 10 from input c to output y. For the case of $\delta = 0$, the same input c and r are obtained and denoted u, i.e., $c = r = u$. In this case, one obtains from Eq. (3) $y = G_o u$, where $G_o = G_c + G_r$. The plots of the magnitudes of G_o are shown in Fig. 11. They indicate that the system follows low-frequency command c, high-frequency command r, and low- and high-frequency command u.

Implementation of the monopulse controller requires its discretization in time. The monopulse signal is supplied with the rate f_d Hz or with the sampling time $T = 1/f_d$ sec. In the case of the DSS-13 antenna, the sampling rate is 10 Hz. A block diagram of the discrete-time monopulse tracker is shown in Fig. 12. The main difference between the continuous-time and the discrete-time trackers lies in a delay of the tracking error.

The monopulse closed-loop systems with sampling rates of 10 and 50 Hz have been simulated. The 50-Hz sampled system has been simulated for evaluation of accuracy of the slower, sampled 10-Hz system. The simulations show similar results for 10- and 50-Hz sampling and are shown in Fig. 8 for the 10-Hz sampled system, where the solid line denotes the tracking error, e, and the dashed line the deviation, δ. The plots show that the pointing accuracy increased more than twofold in both cases. A sampling rate of 10 Hz is satisfactory to maintain the accuracy of the control system, and the 0.1-sec delay does not deteriorate the system performance.

IV. Improving Tracking Performance

As mentioned before, the implementation of the feedforward loop causes a significant excitation of flexible motion of the antenna, specifically in the elevation loop. The mode of deformation for the highest peak in the elevation-to-elevation transfer function is shown in Fig. 13. It is a bending mode of the antenna structure, strongly excited not only by the elevation command but also by the azimuth command. It impacts the stability and performance of an antenna. This mode is extremely difficult to control with elevation and/or azimuth torques, but any one of the following measures can be taken to reduce the impact of this mode on tracking performance: proper location of the elevation pinion, application of a notch filter, or adjustment of the amplifier gain in elevation drive. These measures are described below.

A. Choosing the Elevation Pinion Location

The antenna dynamics for the three positions of the elevation pinion, $\alpha = 0$, 60, and 90 deg, as shown in Fig. 14, have been simulated. The step responses are presented in Fig. 15, showing increased damping of transient motion for the higher location of the pinion. In consequence, the monopulse gains can be increased for the higher pinion, causing smaller tracking errors, as shown in Table 1. The decrease is almost proportional to $\cos\alpha$, which can be explained by the fact that the bending mode is excited mainly by the horizontal component F_h of the elevation pinion force F_t, proportional to the $\cos\alpha$, c.f., Fig. 14.

B. Implementing a Notch Filter

The critical elevation-to-elevation peak can be decreased by applying a notch filter. This narrowband filter removes a component of the specified frequency from the signal. The notch filter transfer function is as follows:

$$G_f(s) = \frac{s^2 + \omega_f^2}{s^2 + 2\delta\omega_f s + \omega_f^2} \tag{8}$$

where ω_f rad/sec is the filter frequency and δ is a damping coefficient which defines the bandwidth of the filter. The elevation input signal to the antenna excites the antenna vibration mode of frequency $f_f = 2.12$ Hz; thus, $\omega_f = 2\pi f_f = 13.32$ rad/sec and $\delta = 0.2$ have been chosen. In implementation, the matching of the filter frequency and the antenna resonance frequency is not a difficult task, since this particular resonance peak is strong and dominant, thus easily detected.

The notch filter is implemented as in Fig. 16. Let (A_f, B_f, C_f, D_f) and (A_r, B_r, C_r, D_r) be the filter and the antenna rate loop state-space representations, respectively. Their transfer functions are shown in Fig. 17, where the 2.12-Hz peak of the rate loop and 2.12-Hz dip of the notch are visible. The state-space representation of the connection is (A_o, B_o, C_o, D_o), where

$$A_o = \begin{bmatrix} A_f & 0 \\ B_r C_f & A_r \end{bmatrix}, \; B_o = \begin{bmatrix} B_f \\ B_r D_f \end{bmatrix},$$

$$C_o = [D_r C_f C_r], \; D_o = D_r D_f \tag{9}$$

and its transfer function is given by the dashed-line plot of Fig. 17. Note that the peak at 2.12 Hz has disappeared. The closed-loop properties of the antenna with and without a notch filter are compared in Fig. 18, where, again, the peak at 2.12 Hz has disappeared. The reduction of the peak allows one to increase significantly the gain of the monopulse loop without losing stability. Figure 19 shows the root locus of the antenna with and without the notch filter, showing that the antenna without the notch filter is stable for the gains $f_m < 0.06$, while the antenna with the notch filter is stable for $f_m < 0.5$. This gain yields about a tenfold reduction in the elevation pointing error, as follows from a comparison of Figs. 20 and 8(a).

Additional simulations have been performed to test the robustness of the system to filter frequency variations up to 10 percent of the nominal frequency, i.e., for filter frequency $f_f = f_{fn} \pm 0.1 f_{fn}$ (and f_{fn} is a nominal frequency). They show negligible deterioration of performance.

C. Adjusting Amplifier Gain

The impact of the critical elevation-to-elevation peak on monopulse controller stability and performance can be reduced by adjusting the open-loop gain. For example, the gain can be adjusted by varying the elevation drive amplifier gain. The elevation drive structure, presented in detail in [7], is shown in Fig. 21. It consists of amplifiers, motors, and gear boxes. The peak level of the elevation-to-elevation mode can be lowered by lowering the gain k_r of the elevation drive to $k_{ro} = \beta k_r$; $\beta = 0.33$ has been chosen through simulated tests. In doing so, the rate-loop transfer function has been lowered for higher frequencies, as in Fig. 22. The feedback gain, which contains an integrator, retains the tracking properties for low frequencies of the closed-loop transfer function, while the higher frequency part of the transfer function is not compensated, lowering the critical peak (Fig. 23). This simple approach allows one to increase gain of the monopulse loop, producing an improvement in tracking performance similar to that with the notch filter in Fig. 20. The explanation is as follows: Let G be the transfer function of the rate loop model from elevation to elevation, and K the transfer function of the PI controller. The closed-loop transfer function G_o is

$$G_o = \frac{KG}{1 + KG} \tag{10}$$

Since K consists of an integrator, therefore $|K| \to \infty$ for $\omega \to 0$, and $|K| \to 0$ for $\omega \to \infty$. It yields $|G_o| \to 1$ for $\omega \to 0$, and $|G_o| \to 0$ for $\omega \to \infty$; thus tracking for low frequencies is preserved, and the peaks in higher frequencies are suppressed. This can be seen in Fig. 23, where the low-frequency part of the closed-loop transfer function is the same, equal to 1 for $\beta = 1$ and $\beta = 0.33$, but for higher frequencies, the transfer function for $\beta = 0.33$ is lower than for $\beta = 1$.

V. Improving SNR

Typically, a monopulse signal is contaminated with measurement noise of significant intensity. Noise intensity is measured with the SNR

$$SNR = 10 \log_{10} \frac{P_s}{P_n} \text{ dB} \tag{11}$$

where P_s and P_n are signal and noise powers, respectively. The noise impacts the pointing accuracy of the control system. Here a simple method that improves SNR is discussed.

The monopulse signal $u(i\Delta t)$ (see Fig. 24) consists of a true measurement $u_o(i\Delta t)$ and a noise $n(i\Delta t)$

$$u(i\Delta t) = u_o(i\Delta t) + n(i\Delta t) \tag{12}$$

where $u_o(i\Delta t) = y_o(i\Delta t) - y(i\Delta t)$. It is assumed initially that the noise $n(i\Delta t)$ is a white noise with zero mean, $E(n(i\Delta t)) = 0$, where $E(.)$ is the expectation operator. The assumption is the worst-case scenario. White noise consists of components of all frequencies of equal intensity s_o, up to the Nyquist frequency f_c, as in Fig. 25(a). Typically, the measurement noise is rather a high-frequency noise; thus its impact on system performance is less severe than that of the white noise.

The monopulse signal $u(i\Delta t)$, shown in Fig. 26 for sampling time $\Delta t = 0.02$ sec, is transmitted to the antenna controller in clusters every N samples (typically $N = 5$); thus the new sampling period is

$$\Delta T = N\Delta t \tag{13}$$

and a cluster $U(i\Delta T) = \{u_1(i\Delta T), u_2(i\Delta T), \cdots, u_N(i\Delta T)\}$, consists of N measurements $u_k(i\Delta T)$

$$u_k(i\Delta T) = u(i\Delta T + k\Delta t),\ k = 1, \cdots, N \tag{14}$$

The mean value, $m_k = E(u_k(i\Delta t))$, and the variance, $\sigma_k = E(\Delta u_k(i\Delta T))^2$, of each component are the same in the cluster

$$m_k = m_N,\ \sigma_k^2 = \sigma_N^2,\ k = 1, \cdots, N \tag{15}$$

This assumption has the following meaning: the value of $u_o(i\Delta t)$ is considered constant within the period ΔT if the reaction of the antenna to $u_o(t_o + i\Delta t)$ is the same as to $u_o(t_o + N\Delta t)$ for $i = 1, \cdots, N$. This property has been confirmed by the earlier simulations reported in [1].

Although the monopulse signal is sent to the controller in clusters, only the last component, $u_N(i\Delta T) = u(i\Delta T + N\Delta t)$, is used to drive the monopulse controller. This excess information is used to reduce the signal-to-noise ratio by averaging the signal within a cluster. The average value, $u_{av}(i\Delta T)$, of the monopulse signal within the cluster of N samples is obtained

$$u_{av}(i\Delta T) = \frac{1}{N}\sum_{k=1}^{N} u_k(i\Delta T) \tag{16}$$

It is shown in the Appendix that in the case of white noise the mean value (m_{av}) of the averaged process, $u_{av}(i\Delta T)$, and the mean value (m_N) of the nonaveraged process, $u_N(i\Delta T)$, are the same, while the variance of the averaged process (σ_{av}^2) is smaller than the variance of the nonaveraged process (σ_N^2) by the factor N

$$m_{av} = m_N,\ \sigma_{av}^2 = \frac{\sigma_N^2}{N} \tag{17}$$

Define r_s, the ratio of variances of nonaveraged and averaged signals, as

$$r_s = \frac{\sigma_N^2}{\sigma_{av}^2} \tag{18a}$$

and its logarithmic counterpart, an SNR increase, ΔSNR, as

$$\Delta SNR = SNR_{av} - SNR = 10\log_{10} r_s \text{ dB} \tag{18b}$$

Then, for white noise, from the definition in Eq. (11), one obtains $r_s = N$ and $\Delta SNR = 10\log_{10} N$ dB.

Consider high-frequency noise with a constant spectrum within the interval $[f_o,\ f_c]$ (see Fig. 25(b)) such that $0 < f_o < f_c$, f_o is a cutoff frequency (the lowest frequency component of the noise), and f_c is the Nyquist frequency, $f_c = 0.5/\Delta t$. Results of noise reduction for the high-frequency noise, obtained through simulations, are shown in Fig. 27. From this plot of the ratio, r_s, versus cutoff frequency, f_o, it is evident that the high-frequency noise is more suppressed through averaging than is the white noise (r_s increases from 5 in the case of white noise to 50 in the case of high-frequency noise for cutoff frequencies of 8 Hz and higher, and SNR increase, ΔSNR, is from 7 to 17 dB, respectively). These results have also been confirmed by simulations of monopulse tracking with $SNR = 20$ dB, where the elevation pointing error for the

case of the nonaveraged signal is shown in Fig. 28(a), and the same error for the averaged signal is shown in Fig. 28(b), with the noise power ratio $r_s = 4.7$ (the SNR increase is $\Delta SNR = 6.7$ dB), which is close to the predicted $r_s = 5$ ($\Delta SNR = 7$ dB).

VI. Conclusions

It has been shown that the feedforward upgrade of the existing DSN antenna servos improves tracking at higher rates, and that monopulse tracking is an appropriate replacement of the conscan technique for the considered rates. A sampling rate of 10 Hz is satisfactory to maintain the accuracy of the monopulse control system, and the 0.1-sec delay does not deteriorate the system performance. Either repositioning of the elevation pinion, implementation of a notch filter, or adjustment of amplifier gain serves as a tool for improving tracking accuracy. The monopulse SNR is improved by averaging the high-frequency sampled signal.

Acknowledgment

The authors would like to thank Ben Parvin for his support and encouragement.

References

[1] W. Gawronski, "Feedforward Control Upgrade of the Deep Space Network Antennas," *The Telecommunications and Data Acquisition Progress Report 42-110, vol. April-June 1992*, Jet Propulsion Laboratory, Pasadena, California, pp. 253–262, August 15, 1992.

[2] D. K. Barton, *Modern Radar System Analysis*, Norwood, Massachusetts: Artech House, 1988.

[3] D. R. Rhodes, *Introduction to Monopulse*, New York: McGraw–Hill, 1959.

[4] J. C. Toomay, *Radar Principles for the Non-Specialist*, New York: Van Nostrand Reinhold, 1989.

[5] G. Biernson, *Optimal Radar Tracking Systems*, New York: Wiley–Interscience, 1990.

[6] J. M. Maciejowski, *Multivariable Feedback Design*, Wokingham, England: Addison–Wesley, 1989.

[7] W. Gawronski and J. A. Mellstrom, "Modeling and Simulations of the DSS 13 Antenna Control System," *The Telecommunications and Data Acquisition Progress Report 42-106, vol. April-June 1991*, Jet Propulsion Laboratory, Pasadena, California, pp. 205–248, August 15, 1991.

Table 1. Pointing errors.

Pinion position, deg	Elevation errors, mdeg	Cross-elevation errors, mdeg	Total errors, mdeg
0	1.43	0.14	1.44
60	0.76	0.08	0.77
90	0.35	0.07	0.36

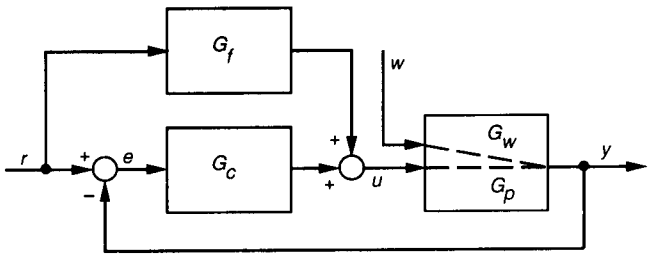

Fig. 1. The PI controller with the feed-forward loop.

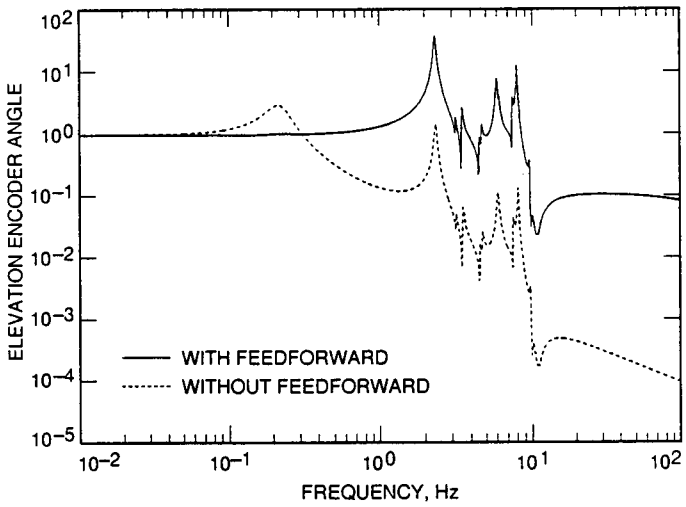

Fig. 2. Magnitudes of the closed-loop transfer function.

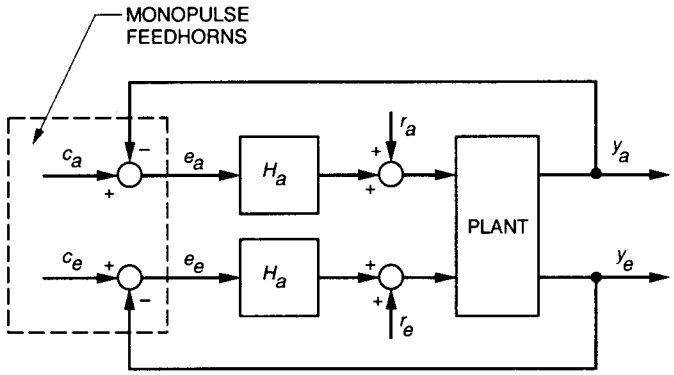

Fig. 4. The monopulse tracking system.

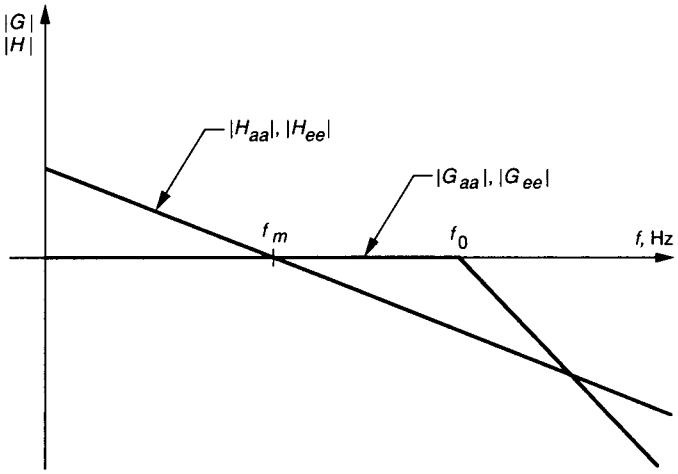

Fig. 5. Magnitudes of *G* and *H*.

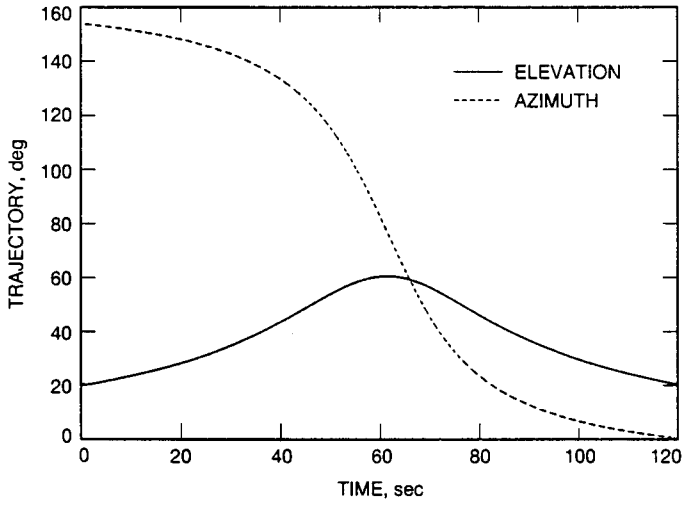

Fig. 3. Elevation and azimuth trajectories.

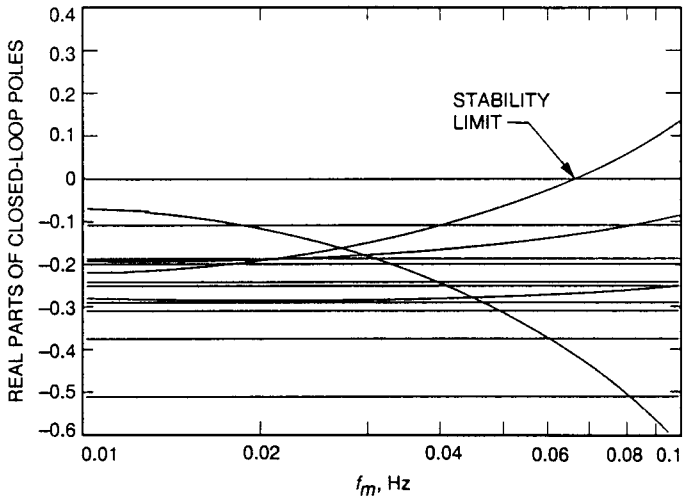

Fig. 6. Real parts of the closed-loop poles versus f_m.

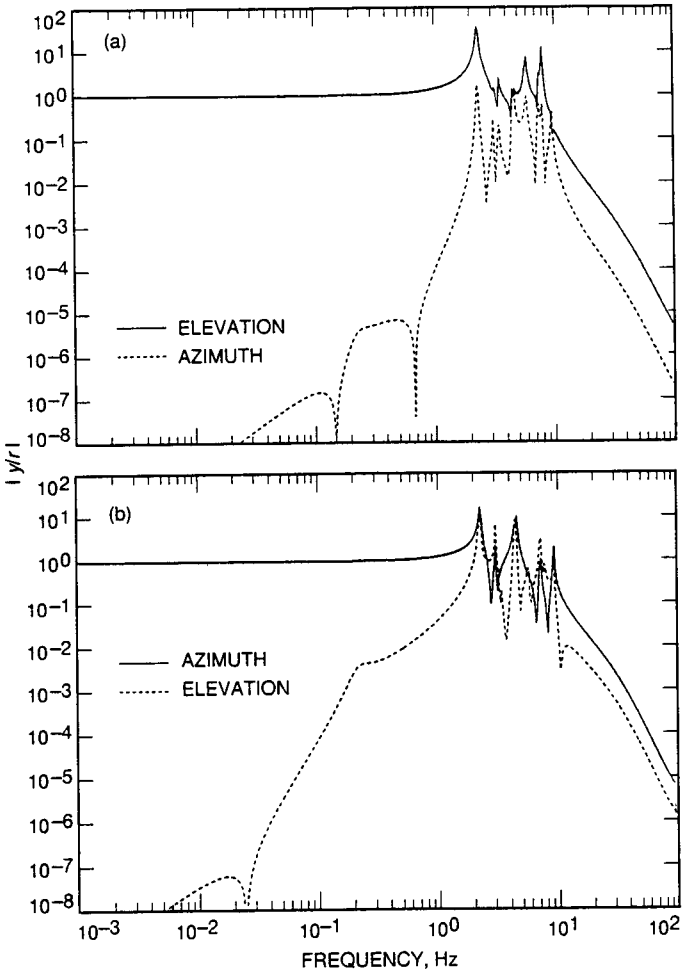

Fig. 7. Magnitudes of the plant transfer function from input *r* to output *y*: (a) elevation angle command and (b) azimuth angle command.

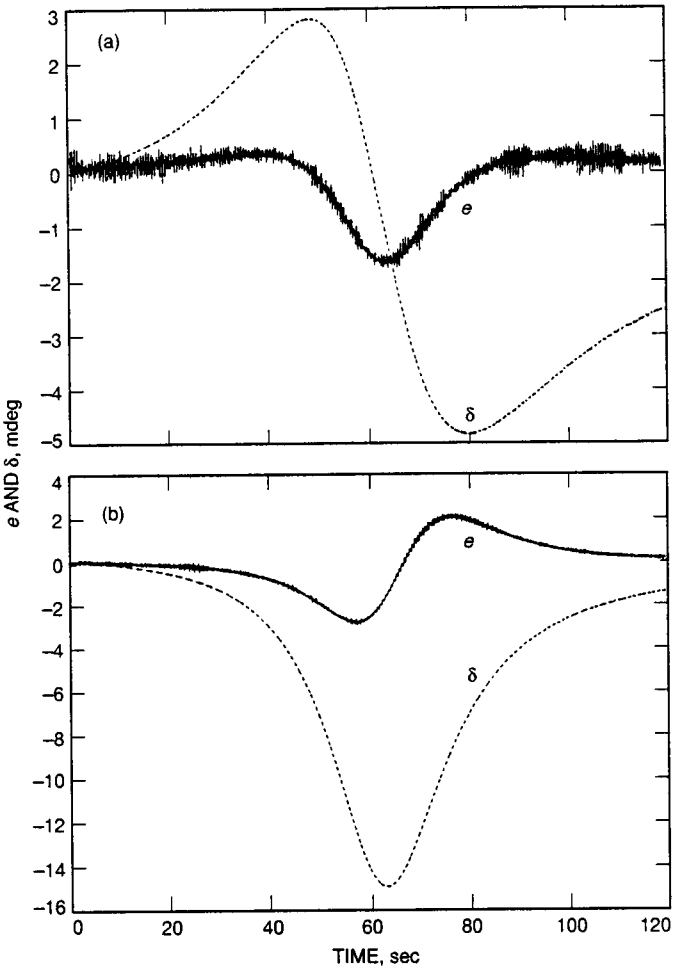

Fig. 8. Tracking error *e* and deviation δ in (a) elevation and (b) azimuth.

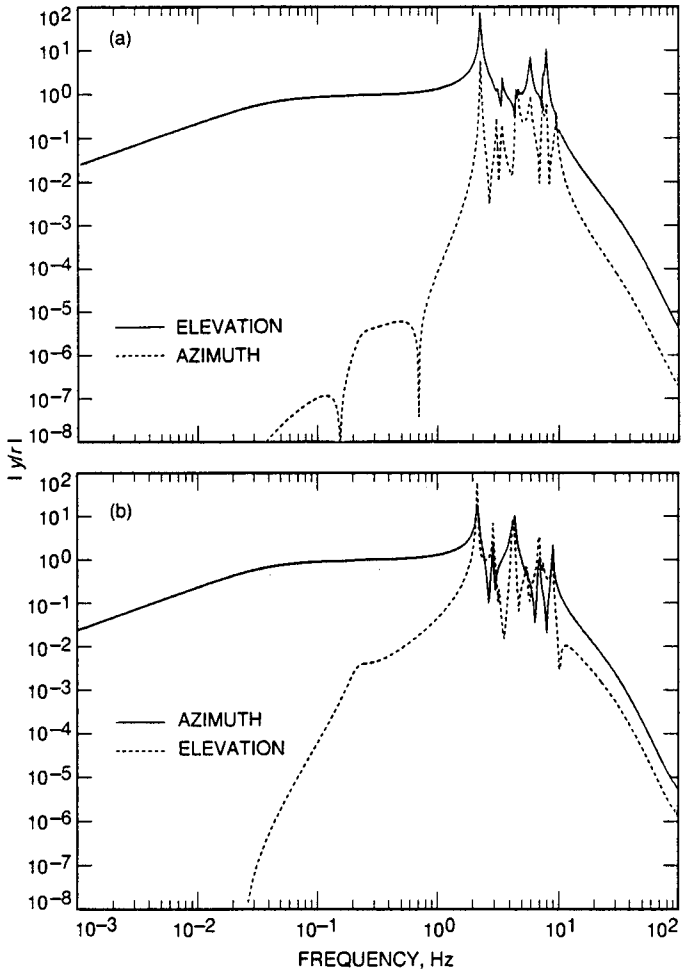

Fig. 9. Magnitudes of the closed-loop transfer function from input *r* to output *y*: a) elevation angle command and b) azimuth angle command.

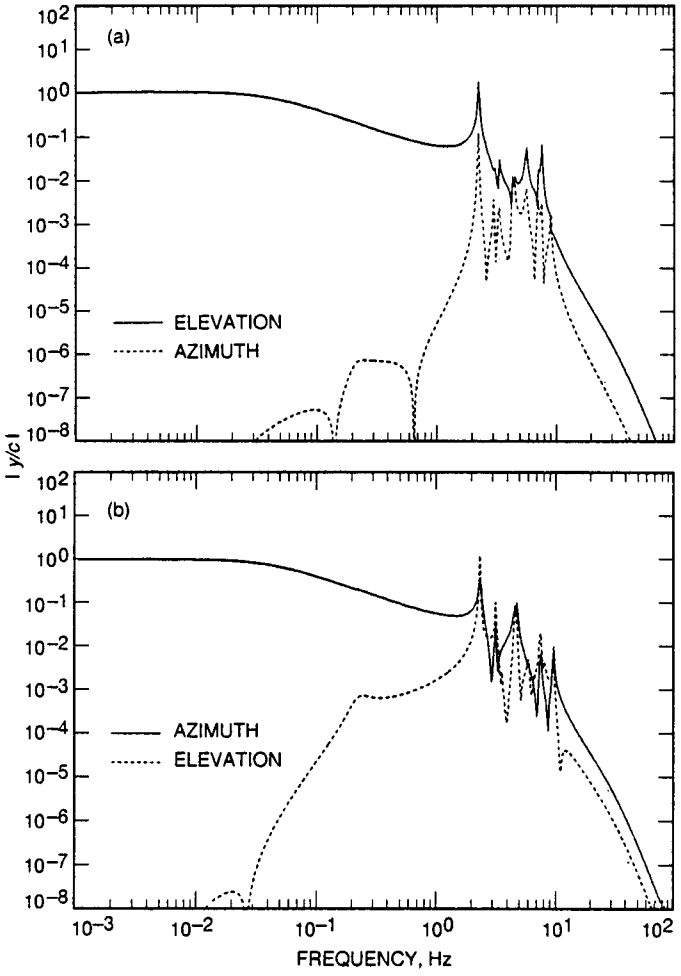

Fig. 10. Magnitudes of the closed-loop transfer function from input *c* to output *y*: (a) elevation angle command and (b) azimuth angle command.

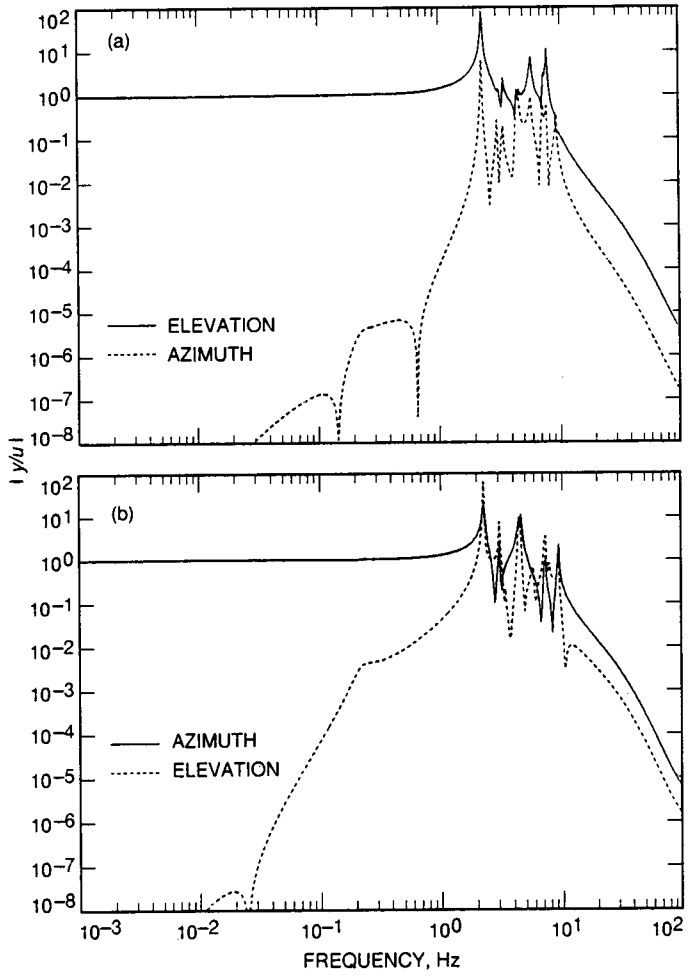

Fig. 11. Magnitudes of the closed-loop transfer function from input $u = c = r$ to output y: (a) elevation angle command and (b) azimuth angle command.

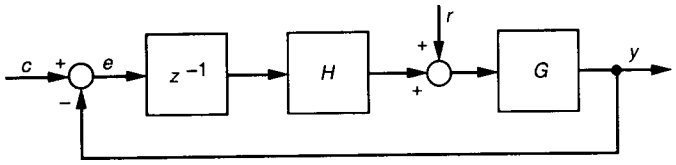

Fig. 12. The discrete-time monopulse tracking system.

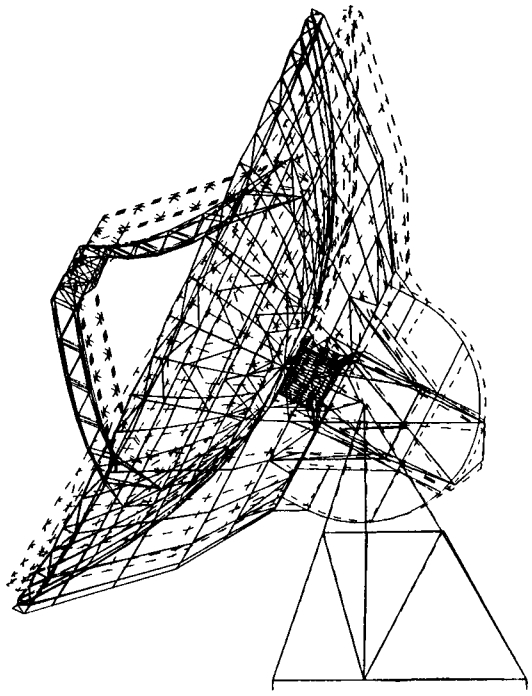

Fig. 13. The bending mode of the antenna.

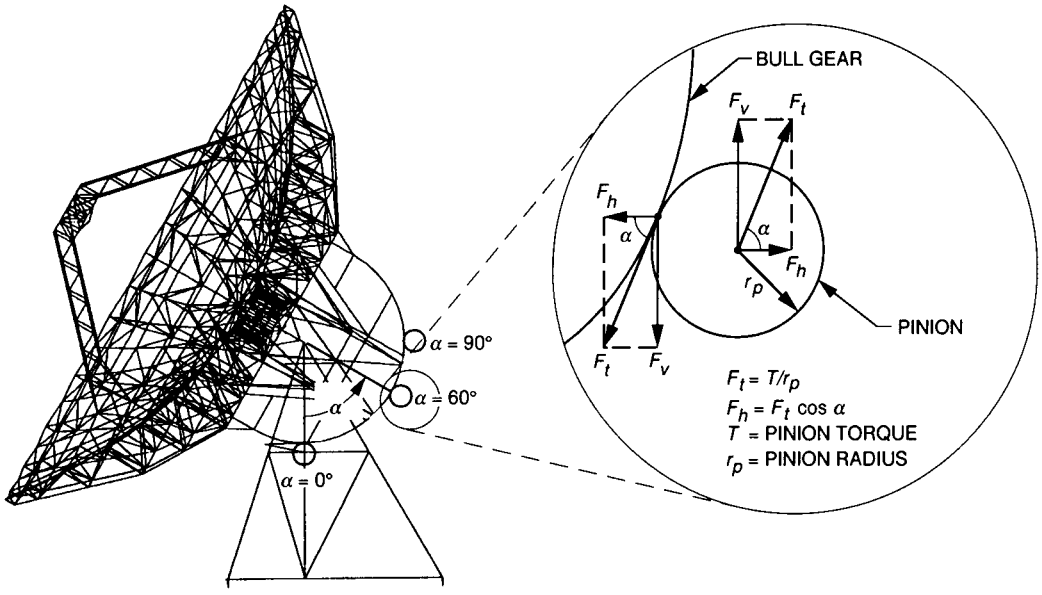

Fig. 14. Elevation pinion locations under investigation.

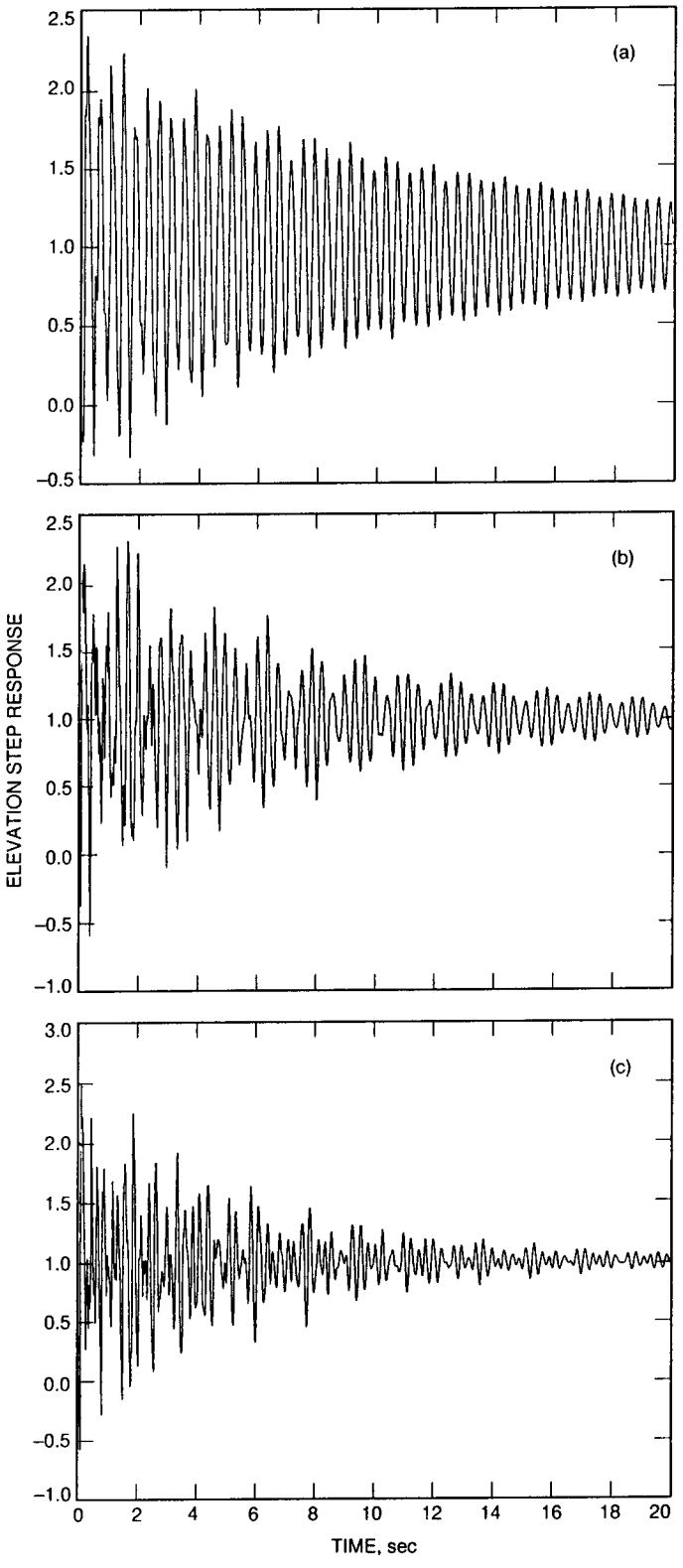

Fig. 15. Step responses (elevation command to elevation encoder) of the closed-loop system, for the elevation pinion at: (a) 0, (b) 60, and (c) 90 deg.

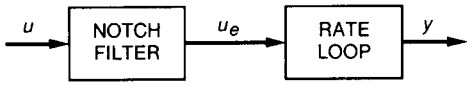

Fig. 16. The rate loop model with a notch filter.

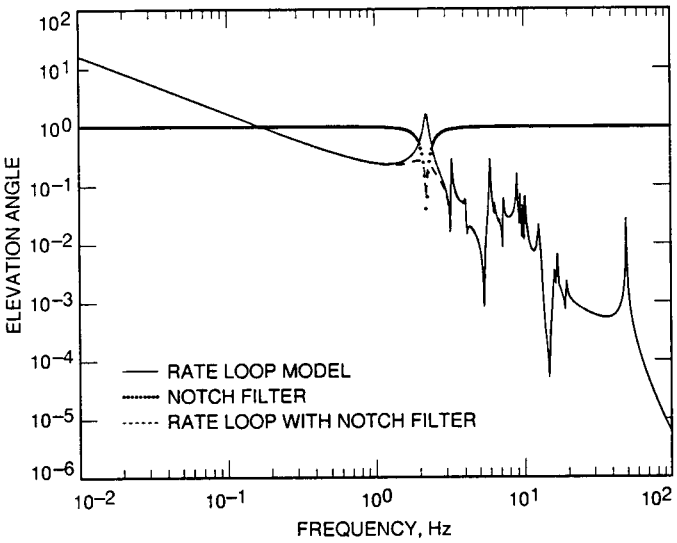

Fig. 17. Transfer functions.

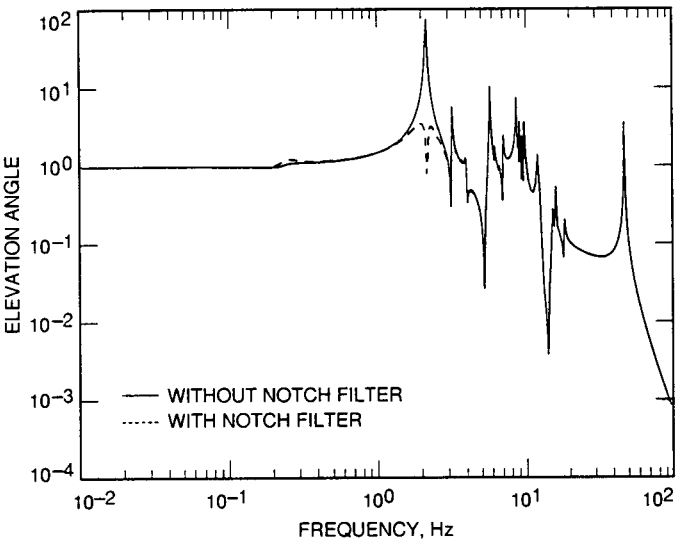

Fig. 18. Transfer functions (elevation command to elevation encoder) of the closed-loop antenna.

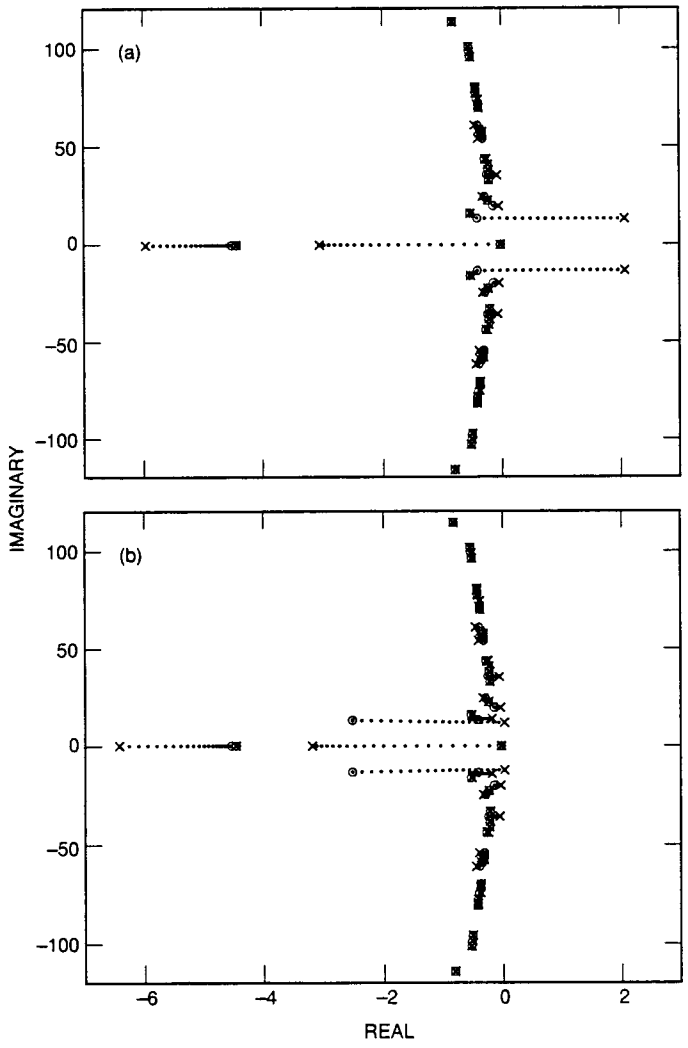

Fig. 19. Root locus of the antenna: (a) without the notch filter and (b) with the notch filter.

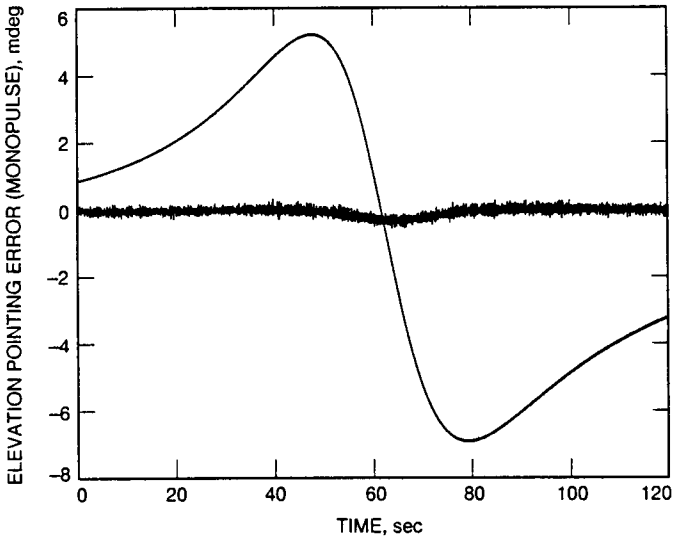

Fig. 20. Elevation pointing error for the antenna with the notch filter.

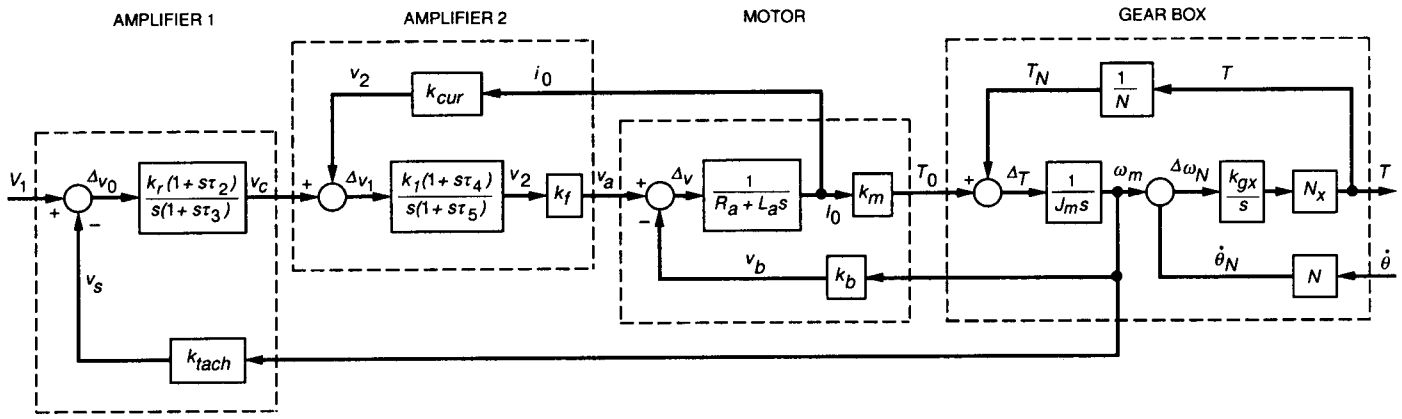

Fig. 21. The elevation drive model.

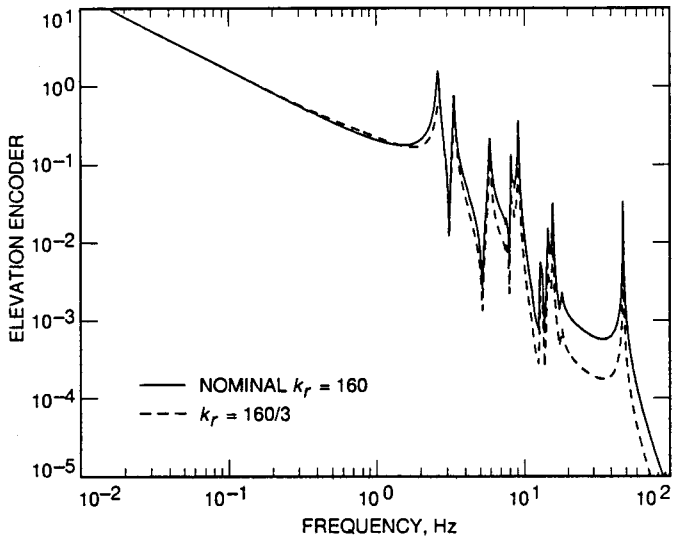

Fig. 22. Transfer functions (elevation rate command to elevation encoder) of the rate loop model.

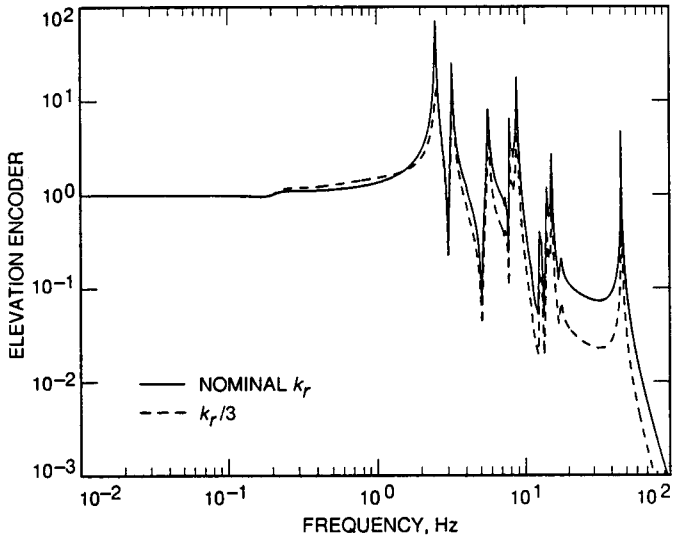

Fig. 23. Transfer functions (elevation command to elevation encoder) of the closed-loop antenna.

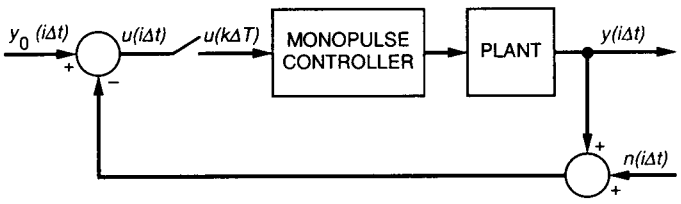

Fig. 24. The monopulse control system.

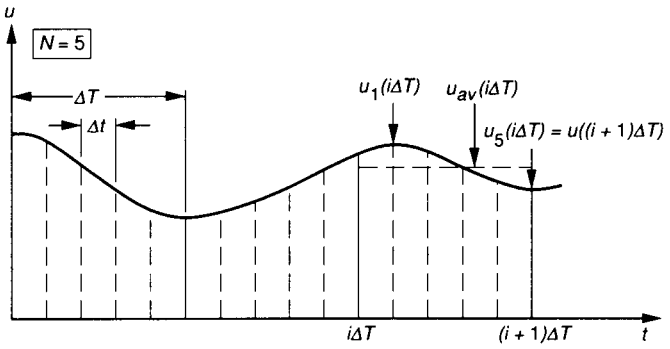

Fig. 26. The monopulse signal.

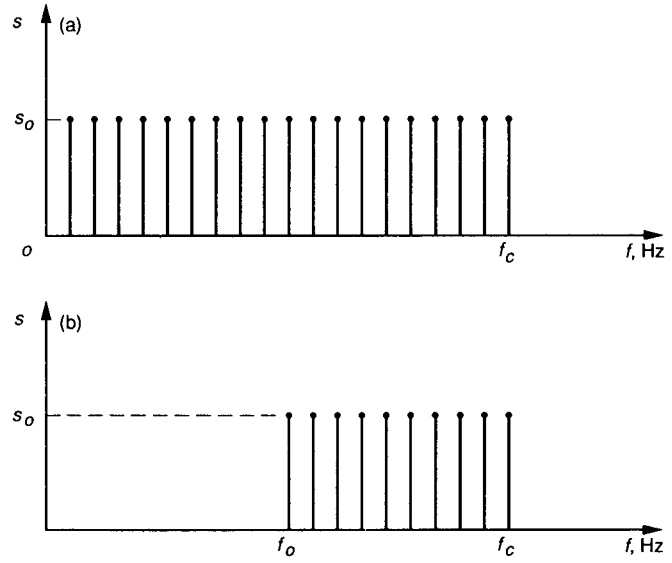

Fig. 25. Spectra of (a) white noise and (b) colored noise.

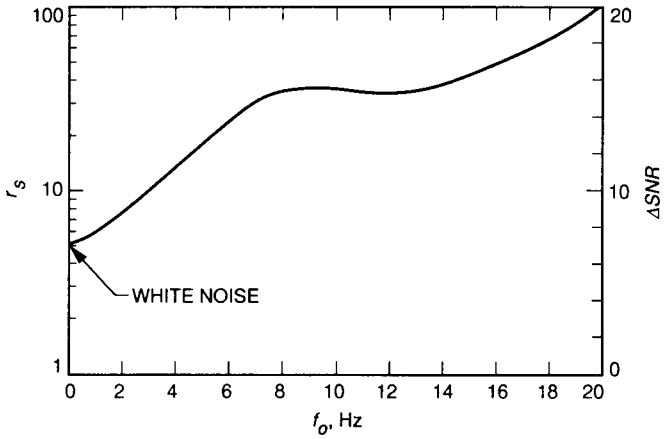

Fig. 27. Variances ratio and SNR increase versus cutoff frequency.

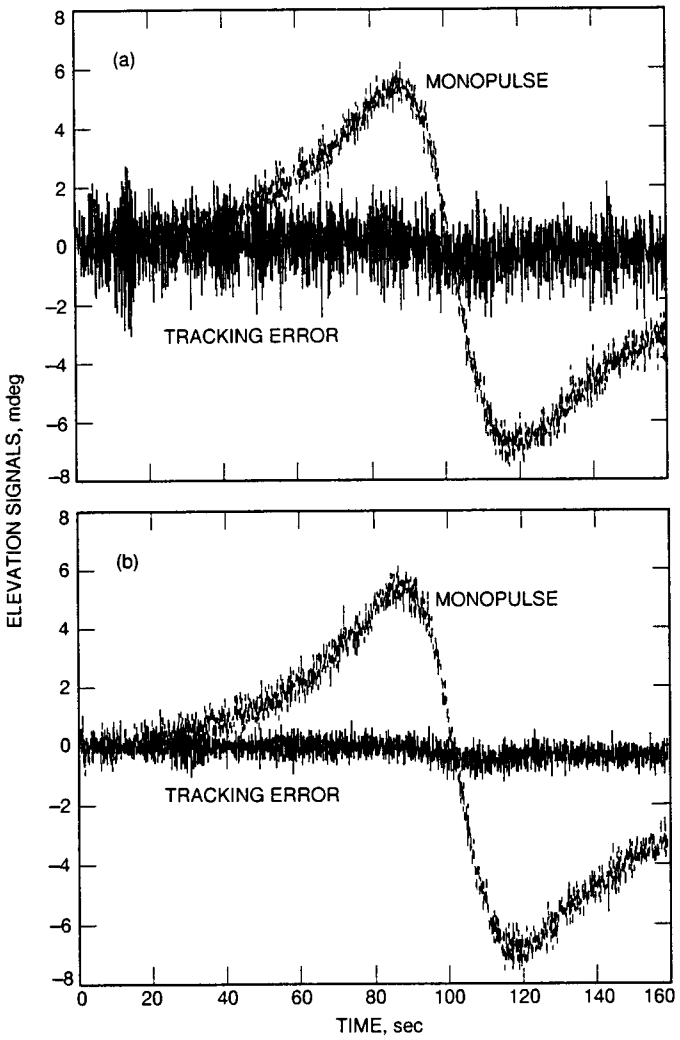

Fig. 28. Elevation tracking error and noisy monopulse signal (a) without averaging and (b) with averaging.

Appendix

Proof of Eq. (17)

The first part of Eq. (17) follows from the definition of the averaged process, Eq. (16), and the equality of mean values in the cluster, Eq. (15). Namely,

$$m_{av} = \frac{1}{N}\sum_{k=1}^{N} E(u_k(i\Delta T)) = \frac{1}{N}\sum_{k=1}^{N} m_k = m_N \tag{A-1}$$

In order to prove the second part of Eq. (17), denote

$$\Delta u_k(i\Delta T) = u_k(i\Delta T) - u_o(N\Delta t) = n_k(i\Delta t) \tag{A-2}$$

$$n_k(i\Delta T) = n(i\Delta T + k\Delta t),\ k = 1,\ \cdots,\ N \tag{A-3}$$

and

$$\Delta u_{av}(i\Delta T) = \frac{1}{N}\sum_{k=1}^{N} \Delta u_k(i\Delta T) \tag{A-4}$$

Thus, the variance of the averaged process is

$$\sigma_{av}^2 = E(\Delta u_{av}(i\Delta T))^2 = \frac{1}{N^2}\sum_{k,l=1}^{N} E(\Delta u_k(i\Delta T)\Delta u_l(i\Delta T)) \tag{A-5}$$

Since the white noise is not correlated, that is

$$E(n_k(i\Delta T)n_l(i\Delta T)) = 0 \quad \text{for } k \neq l \tag{A-6}$$

Therefore

$$E(\Delta u_k(i\Delta T)\Delta u_l(i\Delta T)) = 0 \quad \text{for } k \neq l \tag{A-7}$$

Introducing Eq. (A−7) and Eq. (15) to Eq. (A−5),

$$\sigma_{av}^2 = \frac{1}{N^2}\sum_{k=1}^{N} E\left(\Delta u_k(i\Delta T)\right)^2 = \frac{1}{N^2}\sum_{k=1}^{N} \sigma_k^2 = \frac{\sigma_N^2}{N} \tag{A-8}$$

proves the second part of Eq. (17).